Available online at www.sciencedirect.com
SCIENCE DIRECT®
Applied Surface Science 247 (2005) 243–248
applied surface science
www.elsevier.com/locate/apsusc

Mechanism of ultrashort laser ablation of metals: molecular dynamics simulation

N.N. Nedialkov [a], S.E. Imamova [a], P.A. Atanasov [a,*], P. Berger [b], F. Dausinger [b]

[a] *Institute of Electronics, Bulgarian Academy of Sciences, 72 Tsarigradsko Shose Blvd., Sofia 1784, Bulgaria*
[b] *Institut für Strahlwerkzeuge, Universität Stuttgart, Pfaffenwaldring 43, 70569 Stuttgart, Germany*

Available online 17 February 2005

Abstract

A theoretical model is developed and a molecular dynamics simulation technique is applied for the description of ultrashort laser ablation of metals. The ablation of Al, Ni, and Fe using 0.1, 0.5 and 5 ps laser pulses at wavelengths of 248 and 800 nm is studied. The process is investigated at fluences up to 0.5 J/cm^2. The analysis based on the temporal evolution of the ablation, the temperature, and the pressure distributions into the material reveals that a thermo-mechanical mechanism (spallation) takes place near the threshold. However, phase explosion is found to be the dominant mechanism of material removal at fluences higher than several hundreds of mJ/cm^2. The influence of the laser parameters (wavelength and pulse duration) is obtained and discussed. The ablation depth as a function of the laser fluence and the ablation threshold value are evaluated and compared with the experimental data available. Good agreement between the theory and experiments is observed.

Keywords: Ultrashort laser ablation; Metals; Molecular dynamics simulation

1. Introduction

The rapid development of short-pulsed laser systems over the last decade has offered opportunities for high-precision processing and structuring of wide range of materials—metals [1], semiconductors [2], and organic solids [3]. Besides practical applications of the ultrashort laser pulses, some new fundamental aspects of the laser-beam interactions with matter have been observed.

Laser ablation is a basic mechanism in a large number of laser processing techniques, such as cutting, drilling, surface cleaning, pulsed laser deposition of thin films, etc. It depends strongly on the material's properties and the laser parameters. Its description, however, is complicated by a number of non-thermal processes involved in ultrashort-pulse laser ablation [4].

Several theoretical models have been developed, generally based on heat conduction equations [5], hydrodynamics [6], and molecular dynamics [7,8], which have attempted to bring to light the basic features of the short-pulse laser ablation process. According to these studies, several mechanisms occur,

* Corresponding author.
E-mail address: paatanas@ie.bas.bg (P.A. Atanasov).

0169-4332/$ – see front matter © 2005 Elsevier B.V. All rights reserved.
doi:10.1016/j.apsusc.2005.01.056

depending on the material and the laser parameters. Some authors [3] indicate that the ejection process is caused by the critical pressure gradient, arising in the short time interval after the laser pulse–matter interaction. Thus, the energy is deposited faster than the time it takes for an acoustic wave to form in the system and the relaxation of the pressure gradient created leads to a significant material removal. On the other hand, if the laser pulse duration is shorter than the thermal relaxation time of the system, which is defined by the thermal diffusion, an overheating of the system takes place. Then, the temperature in the material can exceed the critical point and a fast transition to a mixture of liquid and gaseous phase occurs. The estimation of the different ablation mechanisms can be made on the basis of the process trajectory tracing compared with the phase diagram of the given material [9]. Using this method, the ablation in a Lennard–Jones solid is described as a combination of spallation, phase explosion, fragmentation, and evaporation.

In this work, a molecular dynamics (MD) model is developed and applied to study the ultrashort laser ablation of Al, Ni, and Fe. The model reveals the basic features of the ablation of metals by ultrashort laser pulses at relatively low fluences (up to 0.5 J/cm^2). The temporal evolution of the temperature, the pressure distribution in the material, and the ablation depth are presented as a function of the fluence. The theoretical results are compared with the experimental data available.

2. The model

The ablation of metals by ultrashort laser pulses is investigated using the classical molecular dynamics simulation technique [10]. The velocity Verlet algorithm is applied to integrate the equations of motion. The interaction between the atoms in the system is described by the Morse potential as the specific parameters for Al, Ni, and Fe are taken from Ref. [11]. The initial velocities are randomly ascribed to the atoms according to the Maxwellian distribution at room temperature. The ablation is investigated up to several tens of picoseconds. Periodic boundary conditions are applied in the x and y directions of the computational domain in order to simulate an infinite medium. A velocity dampening technique is applied at the bottom of the computational cell in order to prevent the artificial ablation effects that may arise out of the shock wave reflection. The sizes of the computational cell are 6.1 nm × 6.1 nm × 28.4 nm for Al, 5.3 nm × 5.3 nm × 42.2 nm for Ni, and 4.3 nm × 4.3 nm × 37.3 nm for Fe.

The interaction is simulated for pulse durations of τ_p = 0.1, 0.5, and 5 ps and laser wavelengths λ = 248 and 800 nm, respectively. The laser beam intensity is spatially uniform and has a Gaussian temporal distribution. The reflectivity of the metals used in the calculations is given in Table 1 [1,12–14]. It is assumed to be constant during the simulation time interval. The ablation is investigated in vacuum conditions.

The number of photons, corresponding to the laser energy, is deposited into the material exponentially following the Lambert–Beer's law. The energy of the photons is transferred to the atoms of the system within a characteristic time τ_{eq}—the time for electron-lattice energy transfer and establishment of the equilibrium temperature. We obtained the following values of τ_{eq}: 5.3 ps for Al; 5.5 ps for Ni; 5 ps for Fe. These calculations are based on the two-temperature diffusion model [5] with values of the material parameters taken from Ref. [5,15–17]. The energy deposited to the atoms in the system contributes to an increase of their kinetic energy.

The electron thermal diffusion is taken into account in the model as an increase of the effective energy penetration depth. The absorbed energy is deposited into the material within the electron thermal diffusion length. It is calculated by

$$l_{th}^{e} \approx (D_e \tau_{eq})^{1/2} \quad (1)$$

where $D_e = K_e/C_e$ is the electron diffusion coefficient. The values of the electron thermal conductivity K_e and the electron heat capacity C_e and their temperature dependences are estimated in the way described else-

Table 1
Reflectivity of the metals used in the calculations

Material	λ (nm)	R (%)
Ni	248	48
	800	68
Fe	800	65
Al	800	85

where [18]. The electron temperature is estimated on the base of relation obtained by two-temperature diffusion model [5].

Since the electrons are not taken explicitly into account in the presented model, the possible non-thermal mechanisms accompanied the ablation process cannot be described. The non-thermal processes of course will affect qualitatively the ablation process. We have not found any quantitative data in the literature for the contribution of the non-thermal processes in the ablation. However, there are some findings that support the idea that the thermal mechanisms of ablation are dominant above the ablation threshold [1,5].

3. Results and discussion

Snapshots of the atomic configuration in Al, taken at 25 ps after the laser pulse onset at laser fluence $F = 0.2$ and 0.5 J/cm^2 are shown in Fig. 1a and b, respectively. A significant difference can be seen in the structure of the ablated material in the two cases. Fig. 2 represents the distribution of the pressure into the material at different moments after the laser pulse onset for the two fluences in Fig. 1. At 0.2 J/cm^2 (the lower fluence), the absorption of the laser energy leads to the development of thermo-elastic stress that propagates in depth. This stress wave contains a compression component (positive pressure) followed by tension one (negative pressure). A front of tension wave is formed at about 7 nm below the surface of the material (Fig. 2, doted curve). Its amplitude exceeds the strength of the metal, and formation of voids is observed. The process proceeds with coalescence of the voids and formation of a big cluster that leaves the material (Fig. 1a). The ejection, which is driven by thermo-elastic stress formation, is often referred to spallation and it is observed in other materials [3,9].

The increase of the laser fluence results in different characteristics of the ablation. As it is seen, the features of the spallation are not noticed (Fig. 1b). One reason is the change of the thermo-elastic properties of the material with the temperature rise. It results in a decrease of the amplitude of the tension wave developed into the material (Fig. 2, dashed curve), that makes the spallation negligible. Instead of formation of voids and breaks at a certain depth (Fig. 1a), the material starts to decompose homogeneously. At a later stage, the ablated material consists of liquid droplets and single particles (Fig. 1b).

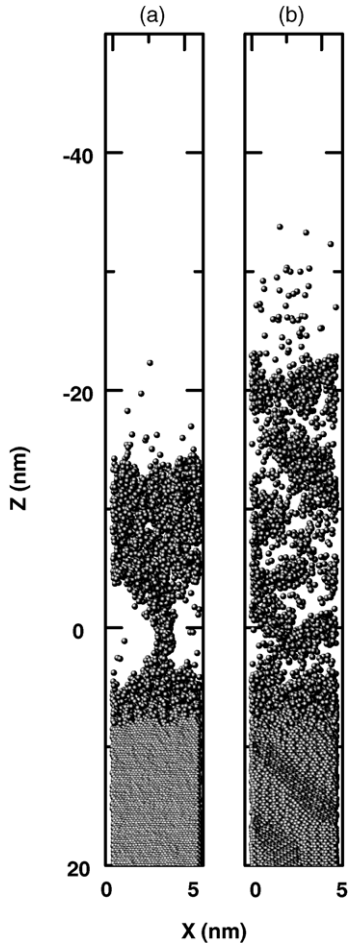

Fig. 1. Snapshots of the atomic configuration in Al at 25 ps after the laser pulse onset: (a) $F = 0.2$ J/cm^2 and (b) $F = 0.5$ J/cm^2. $\lambda = 800$ nm, $\tau_p = 0.1$ ps.

Fig. 3 shows the evolution of the ablation in the temperature–density plane. The solid curve expresses the temperature and density of the material at different moments of the ablation process. The phase diagram of Al [19] is also shown in order to define the different phases of the material. The values for the temperature and the pressure in the material are averaged over the whole absorbing volume. The temperature is calculated from the kinetic energy of the particles with respect to the center of mass. The dotted line in Fig. 3 represents the binodal curve, which defines the

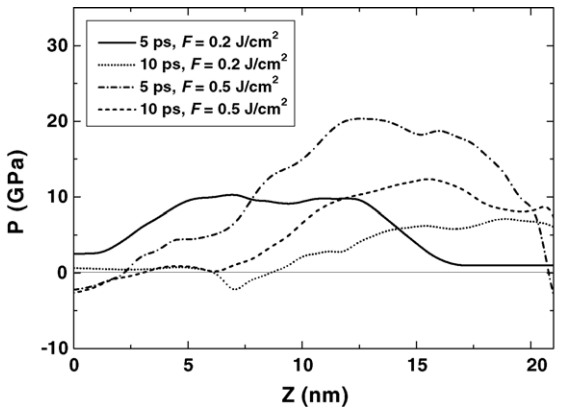

Fig. 2. Depth distribution of the pressure in Al at different moments and fluences. $\lambda = 800$ nm and $\tau_p = 0.1$ ps.

boundary of the area where the liquid and gas phase can coexist. The dashed line (spinodal) corresponds to the boundary where the homogeneous phase is unstable. The energy transfer to the lattice results in a fast heating of the material. As one can see (Fig. 3), the heating can be assumed as taking place in a nearly constant volume. At the end of the heating process (point A), the temperature of the material reaches a value in the order of 10^4 K. The relaxation of the system passes through a fast adiabatic expansion as the temperature decreases. Crossing the binodal curve corresponds to formation of a superheated state, which tends to homogeneously nucleate the gas phase.

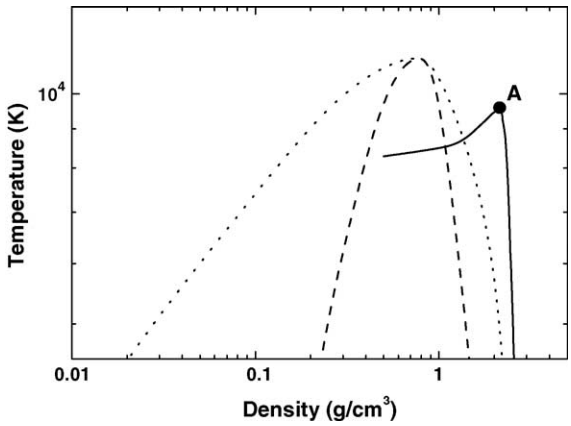

Fig. 3. Evolution of the absorbing volume in Al in the temperature–density plane (solid line). The dashed curve represents the spinodal; the dot curve corresponds to binodal [19]. Point A corresponds to the moments of evolution at 5 ps, after the laser pulse onset. $F = 0.5$ J/cm^2, $\lambda = 800$ nm, and $\tau_p = 0.1$ ps.

Further on, the material decomposes into a mixture of liquid and gas phases (Fig. 1b). This process is referred to as homogeneous boiling or phase explosion [7,9], occurs over the hole absorbing volume, rather than on the surface only (heterogeneous boiling). The evolution of the process continues with a decomposition of the material into well-defined liquid droplets and single particles.

Although the change of the laser wavelength does not affect the basic mechanisms involved in the ablation process, some differences do appear. Fig. 4 represents the evolution of the ablation in Ni at a laser wavelength of 800 nm (a) and at 248 nm (b). The laser fluence in both cases is 0.5 J/cm^2. At the shorter

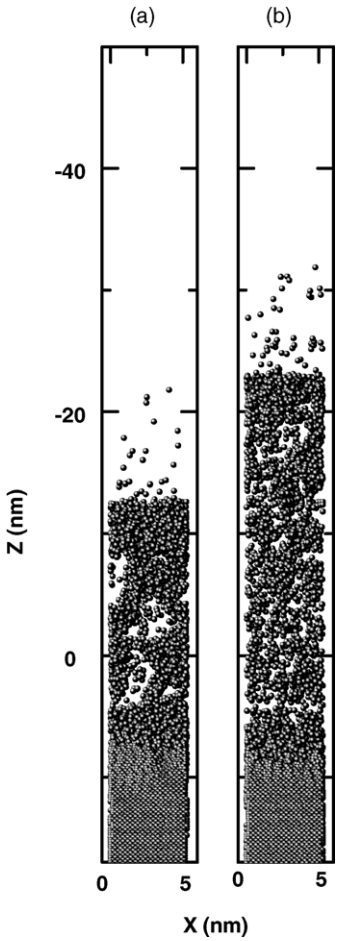

Fig. 4. Snapshots of the atomic configuration for Ni at 25 ps, after the laser pulse onset for: (a) $\lambda = 800$ nm and (b) $\lambda = 248$ nm. $F = 0.5$ J/cm^2 and $\tau_p = 0.1$ ps.

wavelength, a more violent ejection process occurs. The expansion velocity of the overheated material increases by about a factor of two at the UV wavelength, compared to the case of IR laser radiation. Furthermore, the ablated material decomposes faster and contains smaller clusters at the end of the simulation. The shortening of λ is connected with a change of the optical parameters of the material, on the one hand, and to an increase of the photon energy, on the other. As one can see in Table 1, the reflectivity decrease in the UV. Thus, higher energy is deposited into the material and, consequently, a higher volume energy density is reached in the case of UV light compared to that of IR. Due to the stronger heating of the material and higher temperature rate developed, the shock wave formed has higher amplitude and can cause visual structural deformations into the material.

The increase of the laser pulse duration results mainly in a rise of the thermal losses. In the frame of the present work where τ_p is equal to or shorter than the time for electron-lattice energy transfer, observable effects on the process can be related to the contribution of the electron heat diffusion. The increase of the electron heat diffusion depth with the rise of τ_p is found to give a decrease of the maximal achieved temperature (in the case of Fe about 1000 K lower for $\tau_p = 5$ ps compared to $\tau_p = 0.1$ ps at $F = 0.5$ J/cm^2). This effects on the degree of the decomposition of the ablated material as the presence of big clusters in the plume is more pronounced in the case of the longest pulse (5 ps).

The simulation results demonstrate that the ablation of different metals at fixed processing conditions has similar features. The main quantitative differences can be linked to the different properties of the materials investigated. In addition to the optical parameters of the metals (see Table 1), one should also take into account the energetic parameters, such as the cohesion energy. For example, the ablation process in Al and Ni shows some differences at a similar absorbed energy per atom. In case of Al, which has about twice as low cohesion energy as Ni, the decomposition of the material starts earlier and the plume consists mainly of smaller clusters (Fig. 1b and Fig. 4a).

We ascertained the accuracy of the model by comparing of the ablation depths obtained by MD simulation with experimental data. Fig. 5 represents the dependence of the MD-obtained ablation depths

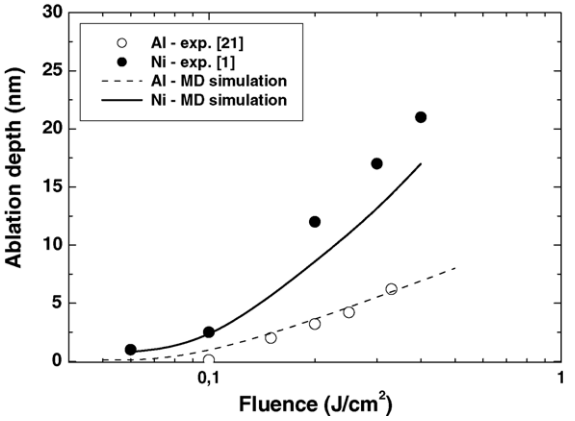

Fig. 5. Ablation depth as a function of the laser fluence for Al and Ni. The experimental data for Al at λ = 800 nm and $\tau_p = 0.1$ ps are taken from Ref. [21] and for Ni at λ = 248 nm and $\tau_p = 0.5$ ps from Ref. [1].

on the laser fluence for Al (dashed curve) and for Ni (solid curve). The depths are estimated from the configuration of the simulated system at the end of the simulation (70 ps). The clear dots in the figures represent the experimental results taken from Ref. [21] for Al and the black dots, those for Ni [1]. As one can see, the comparison shows a good agreement. The values predicted for the ablation threshold—0.085 J/cm^2 for Al and 0.095 J/cm^2 for Ni are also in agreement with the experimental ones—0.105 [21] and 0.085 J/cm^2 [1], respectively. Similar behaviour is obtained for Fe [20].

4. Conclusions

We report results of a MD modeling of ultrashort laser pulse ablation of metals (Al, Ni and Fe) at fluences ranging from the threshold for ablation up to 0.5 J/cm^2. At laser fluences near the ablation threshold, the removal of the material is governed by thermo-elastic stress developing due to a fast heating. Here, the ablated material is composed of big clusters. The increase of the fluence results in a strong overheating of the absorbing volume and a subsequent phase explosion. It leads to decomposition of the ablated material into liquid droplets and single particles.

At the shorter wavelength (248 nm), more violent ejection process occurs compared to the case of IR radiation (800 nm). The expansion velocity of the

overheated material increases by about a factor of two at the UV wavelength, compared to the case of IR laser radiation. Furthermore, the ablated material decomposes faster and contains smaller clusters at the end of the simulation.

The increase of the electron heat diffusion depth with the rise of τ_p is found to give a decrease of the maximal achieved temperature. This effects on the degree of the decomposition of the ablated material as the presence of big clusters in the plume is more pronounced in the case of the longest pulse (5 ps).

In case of Al, which has about twice as low cohesion energy as Ni, the decomposition of the material starts earlier and the plume consists mainly of smaller clusters.

Good agreement between the dependence of the ablation depth on laser fluence and the values of the ablation threshold predicted by the MD model and the experimental data available is observed.

Acknowledgements

This work is supported financially in part by the BMBF Project No. 13N7710/6 (PRIMUS), Germany and by the Bulgarian National Council for Scientific Research under contract F-1209.

References

[1] S. Preuss, A. Demchuk, M. Stuke, Appl. Phys. A 61 (1995) 33.
[2] D. von der Linde, K. Sokolowski-Tinten, Appl. Surf. Sci. 154 (2000) 1.
[3] L.V. Zhigilei, P.B.S. Kodali, B.J. Garrison, J. Phys. Chem. B 102 (1998) 2845.
[4] P.P. Pronko, S.K. Dutta, D. Du, R.K. Singh, J. Appl. Phys. 78 (1995) 6233.
[5] B.N. Chichkov, C. Momma, S. Nolte, F. von Alvensleben, A. Tünnermann, Appl. Phys. A 63 (1996) 109.
[6] R.C. Mancini, Mater. Res. Soc. Symp. Proc. 285 (1993) 63.
[7] L.V. Zhigilei, B.J. Garrison, Appl. Phys. A 69 (1999) S75.
[8] P. Lorazo, L.J. Lewis, M. Meunier, Appl. Surf. Sci. 168 (2000) 276.
[9] D. Perez, L.J. Lewis, Phys. Rev. B 67 (2003) 184102.
[10] M.P. Allen, D.J. Tildesley, Computer Simulation of Liquids, Clarendon, Oxford, 1987, p. 71.
[11] I.A. Girifalco, V.G. Weizer, Phys. Rev. 114 (1959) 687.
[12] D.W. Lynch, W.R. Hunter, in: E.D. Palik (Ed.), Handbook of Optical Constants of Solids, APR, London, 1997, p. 322.
[13] D.W. Lynch, W.R. Hunter, in: E.D. Palik (Ed.), Handbook of Optical Constants of Solids, APR, London, 1997, p. 388.
[14] M.A. Saifi, in: S.S. Charschan (Ed.), Lasers in Industry, Van Nostrand Reinhold Co., New York, 1972, p. 117.
[15] S.-S. Wellershoff, J. Hohlfeld, J. Güdde, E. Matthias, Appl. Phys. A 69 (1999) S99.
[16] I.S. Grigorev, E.Z. Mejlikhov, Fizicheskie Velichini, Energoatomizdat, Moscow, 1991, p. 198.
[17] B.Le. Drogoff, F. Vidal, Y. von Kaenel, M. Chaker, T.W. Johnston, S. Laville, M. Sabsabi, J. Margot, J. Appl. Phys. 89 (2001) 8247.
[18] N.N. Nedialkov, S.E. Imamova, P.A. Atanasov, J. Phys. D 37 (2004) 638.
[19] F. Vidal, T.W. Johnston, S. Laville, O. Barthélemy, M. Chaker, B. Le Drogoff, J. Margot, M. Sabsabi, Phys. Rev. Lett. 86 (2001) 2573.
[20] N.N. Nedialkov, S.E. Imamova, P.A. Atanasov, G. Heusel, D. Breitling, A. Ruf, H. Hügel, F. Dausinger, P. Berger, Thin Solid Films 453C–454C (2004) 496.
[21] M.K. Kim, T. Takao, Y. Oki, M. Maeda, Jpn. J. Appl. Phys. 39 (2000) 6277.